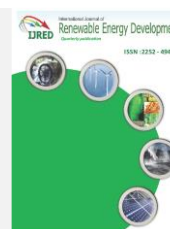




Contents list available at IJRED website

Int. Journal of Renewable Energy Development

Journal homepage: <https://ijred.undip.ac.id>



Research Article

Enhancing Hydrogen Generation using CdS-modified TiO₂ Nanotube Arrays in 2,4,6-Trichlorophenol as a Hole Scavenger

Ratnawati^{a*}, Slamet^b, Farah Diba Toya^b, Satrio Kuntolaksono^a

^a Department of Chemical Engineering, Institut Teknologi Indonesia, Jl. Raya Puspiptek, Serpong, Tangerang, Banten 15320, Indonesia

^b Department of Chemical Engineering, Faculty of Engineering, Universitas Indonesia, Kampus Baru UI, Depok, 16424, Indonesia

Abstract. Nowadays, the lack of renewable energy such as hydrogen, and other environmental issues are problems that must be resolved. 2,4,6-Trichlorophenol (2,4,6-TCP) is classified as a recalcitrant pollutant due to its carcinogenic properties, high toxicity, and dangers to the environment therefore it needs to be eliminated. Hydrogen production using organic pollutant (2,4,6-TCP solution) as a hole scavenger on CdS-TiO₂ nanotube arrays photocatalyst (TNTA-CdS) has been investigated at various CdS loading on TNTA and the initial concentration of 2,4,6-TCP. The TNTA sample was prepared by anodization and followed by an electrodeposition method to decorate CdS on TNTA. The H₂ which was generated by reduction H⁺ and the 2,4,6-TCP removal was performed simultaneously by photocatalysis with TNTA-CdS as photocatalyst. The mole ratio of CdCl₂:CH₃CNSNH₂ as precursors of CdS deposited on TNTA (CdS loading) were 0.1:0.06, 0.2:0.12, and 0.4:0.24 and the initial concentration of 2,4,6-TCP were 10, 20 and 40 ppm. Meanwhile, the photocatalytic performance of the variations in CdS loading on TNTA and initial concentration of 2,4,6-TCP toward hydrogen generation was investigated in a photoreactor for 240 minutes under visible light irradiation with a mercury lamp as a photon source. The CdS decorating on TNTA was confirmed by SEM, EDX, and X-ray diffraction (XRD) characterization. According to the UV-Vis and XRD analysis, the TNTA-CdS samples have bandgap energies in the range of 2.71 - 2.89 eV and comprise a 100% anatase phase. Based on the photocatalysis results, the optimum composition of CdS loading is 0.2:0.16 (TNTA-CdS-2) which produced the highest total hydrogen (2.155 mmol/g) compared to the other compositions and produced 1.5 times higher compared to TNTA at 40 ppm of 2,4,6-TCP.

Keywords: 2,4,6-Trichlorophenol, Hole Scavenger, Hydrogen Evolution, Titania Nanotube Arrays, and TNTA-CdS



@ The author(s). Published by CBIORE. This is an open access article under the CC BY-SA license (<http://creativecommons.org/licenses/by-sa/4.0/>)

Received: 10th March 2022; Revised: 22th June 2022; Accepted: 30th June 2022; Available online: 10th July 2022

1. Introduction

The rising consumption of energy, the severe climate change and other environmental challenges, have necessitated the development of alternative/renewable energy that is environmentally friendly (Li *et al.*, 2020; Tian *et al.*, 2020; Fu *et al.*, 2019). To address these issues of fossil fuel depletion and environmental problems, many efforts have been made toward exploring clean and sustainable energy sources with eco-friendly technologies (Xu *et al.* 2018). The most promising candidate for future energy substitution is hydrogen (H₂) because of its high weight energy density, calorific value, and nonpolluting nature/clean. (Junn Ng *et al.*, 2020; Luo *et al.*, 2020). Currently, a variety of feedstocks have been used to produce hydrogen, including fossil resources, for instance, coal and natural gas, as well as renewable resources such as water and biomass. Numerous process technologies have been reported for hydrogen generation, including biological (Holladay *et al.*, 2009), electrolytic (Liu *et al.*, 2020), photocatalytic (Shi *et al.*, 2020), and thermochemical (Mehrpooya *et al.*, 2020) processes. These

processes are at various stages of development, each offering unique opportunities, benefits, and challenges.

Photocatalysis is a chemical process induced by photo-irradiation in the presence of a photocatalyst. This process is based on a simple concept, where the illumination photon with energy above the photocatalyst's bandgap excites electrons/e⁻ from the valence band (VB) to the conduction band (CB). Consequently, generating holes/h⁺ in the VB. This photo-induced h⁺ and e⁻ produce oxidation and reduction reaction of chemical species adsorbed on the photocatalyst surface unless they recombine to prevent the redox reaction. Recently, photocatalytic H₂ generation has been mainly used to produce renewable clean fuels which can achieve zero-emission (Christoforidis *et al.*, 2018). Numerous studies have attempted to synthesize semiconductor photocatalysts to achieve efficient photocatalytic hydrogen production (Zhao *et al.*, 2018; Zheng *et al.*, 2020).

CdS, a narrow bandgap (2.45 eV) and narrow conduction band edge positions semiconductor, is one of the promising photocatalysts in hydrogen production (Gholipour *et al.*, 2015). Furthermore, CdS can reduce

* Corresponding author:
Email: mwt63@yahoo.co.id (Ratnawati)

protons/H⁺ to H₂ due to the absorption of visible light with a long wavelength in photocatalysis which is not limited to its application to solar photocatalysis. However, this photocatalyst has drawbacks such as its instability under irradiation, a small bandgap leading to the recombination of photoexcited electrons-holes, as well as high susceptibility to corrosion by excited holes (Gholipour *et al.*, 2015; Zhao *et al.*, 2016). Therefore, pure CdS must be combined with other semiconductors to overcome these limitations. For this reason, several studies, including morphological control (Wang *et al.*, 2018; Zhao *et al.*, 2019) and modification (Ba *et al.*, 2019) have been carried out to enhance the photocatalytic performance of CdS.

Nowadays, titanium dioxide (TiO₂) was the most common and promising photocatalyst used in hydrogen production (Slamet *et al.*, 2017; Zhao *et al.*, 2016), waste minimalization (Elangovan *et al.*, 2021; Sharotri *et al.*, 2016), dye-sensitized solar cells (Zhao *et al.*, 2016). It is commonly used as a semiconductor due to the compound's stability, pollutant-free nature, availability in nature, inexpensiveness, and resistance to corrosion (Acar *et al.*, 2016). In photocatalytic H₂ generation, several processes have been performed to enhance the utilization efficiency of TiO₂ photocatalyst under visible light, increase the surface area and reduce the electron-hole recombination. These processes include depositing with nonmetal and metal ions to be active with visible light and reducing the recombination of photogenerated e⁻ and h⁺ (Sharotri *et al.*, 2016; Slamet *et al.*, 2017), getting morphology modifications in the forms of nanotubes (Elysabeth *et al.*, 2021), and combining with narrow bandgap semiconductors such as CdS (Tian *et al.*, 2015; Zhao *et al.*, 2016). TiO₂-CdS is a common composite system.

CdS modified with TiO₂ nanoparticle or TiO₂ nanotube arrays (TNTA) as a semiconductor has shown remarkable performances in the field of photocatalytic performance. For instance, several studies using TiO₂/TNTA-CdS for H₂ production (Junn Ng *et al.*, 2020; Wang *et al.*, 2014; Zhao *et al.*, 2016; Zhu *et al.*, 2015), methane production (Park *et al.*, 2016), and for degrading dye and diclofenac pollutants (Elangovan *et al.*, 2021; Li *et al.*, 2015). This photocatalyst was selected to minimize the recombination and enhance the activating response to visible light. The presence of CdS on TNTA increased the mechanical stability and produced more hydrogen (Liu *et al.*, 2011). TiO₂ with the morphology of nanotube arrays produced by the anodizing process is widely used due to the high surface area (Elizabeth *et al.*, 2021; Slamet *et al.*, 2017).

Numerous reports have shown organic compounds containing hole scavengers tend to reduce recombination and serve as H₂ source to enhance hydrogen generation through oxidation reaction (Luo *et al.*, 2009; Slamet *et al.*, 2017). Examples of organic compounds containing hole scavengers include glycerol (Slamet *et al.*, 2017), methanol (Levy *et al.*, 2012), and ethanol (Hippargi *et al.*, 2018). Furthermore, 2,4,6 TCP, a hazardous pollutant, is also a suitable hole scavenger/sacrificial agent for H₂ production. This process could help in eliminating waste while producing renewable energy. 2,4,6-TCP needs to be degraded since it causes carcinogenic effects and is dangerously toxic for life even at low concentrations. According to International Agency for Research on Cancer (IARC), it is categorized as carcinogenic 2B Group (Ali *et al.*, 2019). This waste comes from pharmaceutical, petrochemical, textile, and pesticide waste. Some studies have been performed to photodegrade 2,4,6-TCP using TiO₂/graphene (Ali *et al.*, 2019), MgO-MgFe₂O₄ (Ramirez *et*

al., 2019), CdS (Khodadadeh *et al.*, 2016), TiO₂-Carbon (Lavand *et al.*, 2015), and g-C₃H₄ (Ji *et al.*, 2013). In addition, biological degradation, coagulation, adsorption, and AOP method were also performed to eliminate 2,4,6-TCP (Ali *et al.*, 2019; Khorshandi *et al.*, 2018). However, 2,4,6-TCP can present an attractive renewable material that can be degraded and converted to H₂ simultaneously. Therefore, this would be profitable as a new source for H₂ production and waste reduction. Few studies have been conducted for hydrogen production using TNTA-CdS and degrading 2,4,6-TCP either separately or simultaneously. H₂ production and 2,4,6-TCP degradation simultaneously has been performed previously using TiO₂ nanotube/graphene composite (Slamet *et al.*, 2017). Unfortunately, the application of TNTA-CdS composite in hydrogen production and degrading with 2,4,6 TCP simultaneously has not been studied in detail.

This study reports a combination of degradation and H₂ production using TNTA-CdS photocatalyst with 2,4,6-TCP as a hole scavenger. Modification of TNTA with CdS was carried out by the electrodeposition process. Subsequently, the TNTA-CdS was characterized by SEM-EDX, XRD, and UV-Vis DRS analyses. The effect of loading CdS on TNTA, and the initial concentration of 2,4,6 TCP in H₂ generation were also evaluated.

2. Materials and Methods

2.1. Materials

Nitric acid (HNO₃, 65%), 2,4,6 Trichlorophenol (2,4,6 TCP, 98%), and hydrofluoric acid (HF, 65%) were purchased from Merk. Furthermore, Glycerol solution (98,8%) was procured from Brataco, while thioacetamide (CH₃CSNH₂, 98%) and cadmium chloride (CdCl₂, 99%) were obtained from Sigma Aldrich. All the chemicals used without further purification and the aqueous solutions were prepared using distilled water.

2.2. Preparation of TNTA

Titanium foils (0.3 mm thickness, 99.6%) were mechanically polished with sand using cc1500cw, chemically polished for 2 minutes with a mixture of HF, HNO₃, and H₂O (1:3:6), rinsed with deionized water, then dried. The anodization process was performed using Pt electrode (2 mm thickness) as the cathode and Ti foils as the anode, in an electrochemical cell equipped with a DC power supply (ESCORT 6030SD). At room temperature, the Ti foils were anodized for 2 hours at 50 V in a 60 ml glycerol electrolyte solution containing 0.5 wt% NH₄F and 25 wt% water, with continuous stirring at 150 rpm (NESCO79-1A) to produce TNTA. Subsequently, the TNTA was rinsed with deionized water and calcined for 3 hours at 500°C in an atmospheric furnace as previously reported with slight modification (Ratnawati *et al.*, 2014).

2.3. Modification of TNTA with CdS

TNTA-CdS was prepared through electrodeposition in a TPC 015 ultrasonic bath, where Pt electrode and TNTA served as the anode and cathode, respectively. The electrolyte contained CdCl₂ and CH₃CSNH₂ in various mole per Liter ratios, to obtain TNTA-CdS-1 (0.1:0.06), TNTA-CdS-2 (0.2:0.12), and TNTA-CdS-3 (0.4:0.24). Furthermore, the electrodeposition process was performed at 1.5 V for 0.5 hours. Subsequently, the TNTA-CdS

produced was washed with distilled water and annealed for 2 hours at 350°C in an atmospheric furnace.

2.4. Characterization of catalyst

The morphological structure of TNTA-CdS was evaluated using a Scanning Electron Microscope (SEM, JSM-6510LA) equipped with an energy dispersive X-ray analyzer (EDX) to know the elemental composition. The energy bandgap of the photocatalyst produced was measured using UV-Vis diffuse reflectance spectra (UV-Vis DRS) analysis (Shimadzu 2450 Spectrophotometer). The samples' absorbance and reflectance were then determined at ambient conditions in the wavelength of 200 to 600 nm. To evaluate the photocatalyst's crystalline phase, X-ray diffraction (Shimadzu 7000 X-ray diffractometer) was used at 40 kV and 30 mA with Cu K α ($\lambda = 0.154184$ nm). Meanwhile, the Scherrer equation was employed to calculate the crystallite sizes of the TNTS-CdS estimated from full width at half-maximum (FWHM) (Slamet *et al.*, 2017).

2.5. Photocatalytic Hydrogen Production

The photocatalyst's activity was investigated for hydrogen production from the reactant (200 mL of 2,4,6-Trichlorophenol solution) through the photocatalysis reaction conducted in a 500 mL Pyrex glass reactor equipped with two mercury lamps (Philips HPL-N 250 W/542 E40 HG ISL with 83% visible light and 17% UV) as a photon source to stimulate the reaction, as well as a magnetic stirrer to homogenize the reactant. The mercury lamps were then placed 1 cm away from the photoreactor, and the photocatalytic reactor system was placed in a reflector box for 4 hour-irradiation. Before the irradiation, the TNTA-CdS in reactant within the reactor flask was magnetically stirred and purged with argon to eliminate air that could hamper the H₂ generation and to test the photoreactor's leakage. The photoreactor is equipped with a cooling system in the form of 2 exhaust fans which are placed on the walls of the reflector box, and after 75 minutes of irradiation, the temperature became constant around 80°C.

Subsequently, the H₂ produced was analyzed by online sampling every 30 min using Gas Chromatograph (Shimadzu GC 2014) equipped with a molecular sieve (MS Hydrogen 5A, 80 - 100 mesh) column for hydrogen analysis which was connected to a personal computer.

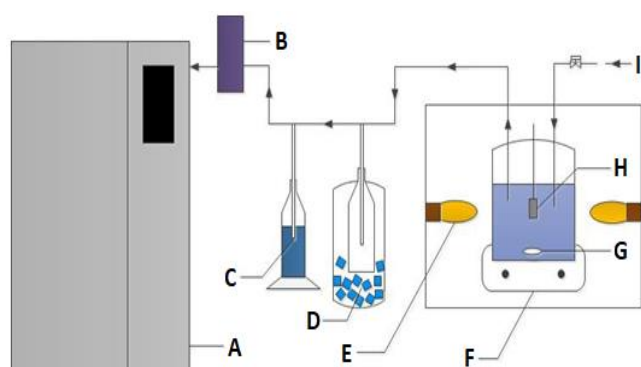


Fig. 1. The schematic diagram of the photocatalytic reactor: A. Gas chromatograph, B. Injector, C. Secondary water trap, D. Primary water trap, E. Mercury lamp, F. Magnetic Stirrer, G. Magnetic Bar, H. Photocatalyst, and I Argon Gas.

Meanwhile, the signal/peak of hydrogen was recorded using a Thermal Conductivity Detector (TCD) system with high purity argon/Ar (99.99%) at 50 cm³ min⁻¹, as a carrier gas. Figure 1 presents a schematic diagram of the photoreactor.

3. Results and Discussion

3.1. Semiconductor Analysis

The present study investigates the morphological analysis of TNTA-CdS using scanning electron microscope (SEM) imaging. The SEM images in Figures 2a and 2b show the TNTA were regularly and perpendicularly self-organized. Meanwhile, Figure 2c confirms the presence of CdS on the surface of the tube which tends to be brittle due to sonication in the modification process. According to the Figure, CdS nanoparticles are deposited on the TNTA surface and some CdS nanoparticles are observed outside the nanotubular structures (the space between the tubes). This result is in line with the reports of previous studies (Liu *et al.*, 2011; Xie *et al.*, 2016). Based on the EDX analysis on TNTA, the components detected were Ti, O, C, F, Cd, and S (Table 1). The C, N, and F were obtained from glycerol and NH₄F (Slamet *et al.*, 2017), however, for TNTA-CdS, there are additional components: Cd and S. The mass percentage of Cd was much larger, compared to S, indicating Cd²⁺ formed compounds other than CdS. These results confirmed CdS was successfully deposited on TNTA. The diameter ranges for TNTA and TNTA-CdS-2 were 123-144 nm and 130-152 nm, respectively, while the tube thickness was 25-27 nm and 22-28 nm, respectively. According to the previous study, the tube height of TNTA formed after anodizing and annealing with air was about 1500 nm (Slamet *et al.*, 2017). The competition between chemical dissolution within the tube's mouth and inside wall and the oxidation reaction at the tube's bottom, influence the highly ordered morphology of TNTA.

UV-Vis diffuse reflectance spectra (DRS) were recorded to investigate the TNTA's light absorption ability and the variations of TNTA-CdS. In comparison with bare TNTA, the light absorbance edge of TNTA-CdS-1, TNTA-CdS-2, and TNTA-CdS-3 photocatalyst were significantly red-shifted to the visible region (Figure 3). This is possibly due to the decorating of CdS on TNTA, which has been reported to improve the visible light capability of TNTA-CdS (Elangovan *et al.*, 2021; Li *et al.*, 2015). By extrapolating the Tauc plot of the transformation of Kubelka-Munk $[F(R) \cdot hv]^{1/2}$ vs energy (hv) in the linear section and intersecting on the x-axis, the bandgap of photocatalyst can be evaluated (Elangovan *et al.*, 2021), with F(R) according to equation 1.

Table 1
The Elemental composition of TNTA and TNTA-CdS-2

Component	%mass	
	TNTA	TNTA-CdS-2
Ti	63.87	50.16
O	32.95	28.08
C	0.71	1.17
N	1.65	1.22
F	0.83	0.37
Cd	-	18.71
S	-	0.34

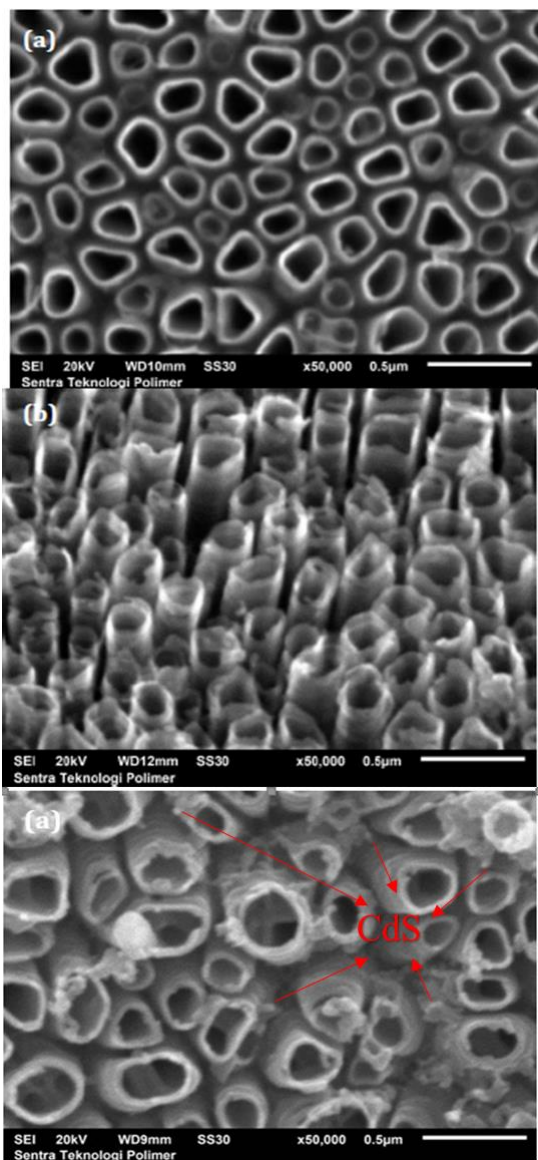


Fig. 2. The SEM image for (a) TNTA from the top, (b) TNTA at an angle of 45°, (c) TNTA-CdS-2 from the top at 50.000x magnification.

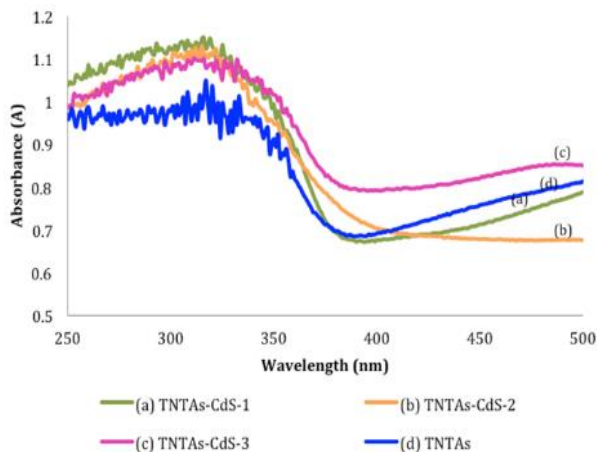


Fig. 3. The DRS spectra of bare TNTA and variations of TNTA-CdS photocatalysts.

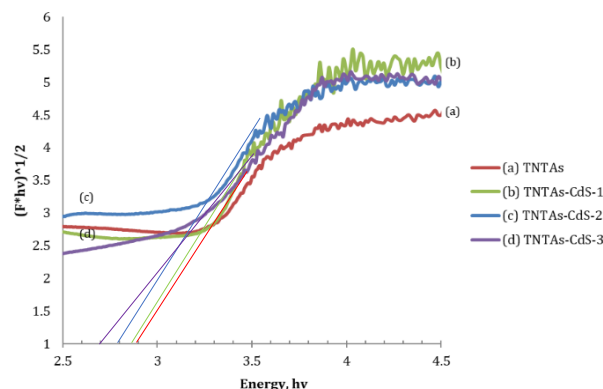


Fig. 4. The T_{auc} plot for determination of bandgap of photocatalyst samples.

$$F(R) = [(1-R)^2/2R] \tag{1}$$

Where R is the converted reflectance (%) of the UV adsorption spectra, h = plank’s constant, v = frequency.

The Tauc plot of transformed Kubelka-Munk function vs energy (eV) for various TNTA-CdS photocatalysts for calculation of bandgap is presented in Figure 4, and the evaluation of the bandgap is using indirect band gap (Chen *et al.*, 2013).

Based on Figure 4, the bandgap of TNTA, TNTA-CdS-1, TNTA-CdS-2, and TNTA-CdS-3 was found to be 2.91, 2.89, 2.8, and 2.71 eV, respectively. This means CdS deposited in TNTA modifies the photocatalyst due to a reduction in the bandgap energy. Therefore, higher CdS loading on TNTA will result in even lower bandgap energy due to the low bandgap of CdS (2.45 eV). This is in line with the report of the previous studies (Li *et al.*, 2015). The enhanced ability of the TNTA-CdS in absorbing visible light makes the composite potentially suitable for solar-driven applications.

Figure 5 depicts the XRD patterns of TNTA and TNTA-CdS-2 samples. The diffraction peak observed at $2\theta = 25.3^\circ, 37.80^\circ, 48^\circ, 54.3^\circ,$ and 55.05° indicates anatase crystals of TNTA derived from (101), (004), (200), (105), and (221) crystallite orientations (JCPDS no 21-1272). However, there is no indication of rutile phase of TNTA because there were no diffraction peaks at $2\theta = 27.4^\circ$ and 36° (JCPDS No.21-1276) (Slamet *et al.*, 2017). Furthermore, after depositing, TNTA-CdS-2 exhibited a weak diffraction peak at around $2\theta = 43.7^\circ$ assigned to the (110) plane of hexagonal phase CdS according to JCPDS#41-1049 (Xie *et al.*, 2016, Yu *et al.*, 2021). These results confirm the successful decoration of CdS on the TNTA surface, which is in accordance with the SEM and EDX results. Also, the diffraction peaks at around $2\theta = 23.6^\circ, 30.56^\circ$ and 50.12° indicate the presence of $CdCO_3$ impurities formed during the electrodeposition process (JCPDS = No.Data 421342) (Moreira *et al.*, 2017, Veeraputhiran *et al.*, 2017). The anatase crystal size of TNTA and TNTA-CdS-2 were discovered to be 20.4 and 27.17 nm, respectively, using Scherrer’s equation (Li *et al.*, 2015; Slamet *et al.*, 2017). This shows depositing with CdS led to a significant increase in the crystal size. The calcination temperature and duration also play an important role in enhancing the crystalline anatase phase (Aphairaj *et al.*, 2011).

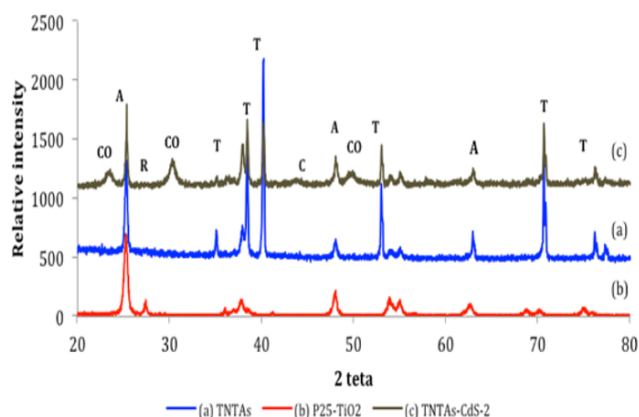


Fig. 5. The XRD patterns of bare TNTA, TNTA-CdS-2 and TiO_2 -P25 photocatalysts where T = Ti, A = Anatase, R = Rutile, C = CdS, CO = CdCO_3 .

In the synthesis of TNTA-CdS, there were 2 calcination processes, which were at 500 °C for 3 hours and at 350°C for 2 hours. This caused the increase of anatase crystals; however, no rutile crystals were identified. Therefore, the CdS depositing on TNTA enhanced the diffraction and crystallinity (Li *et al.*, 2015).

3.2. Hydrogen Production and 2,4,6 TCP elimination

In terms of morphology, TNTA reportedly produces 5 times more hydrogen, compared to P25- TiO_2 , considering the two photocatalysts produced 1.503 and 0.298 mmol/g of H_2 , respectively (data not presented). This is because the neat arrangement of TNTA tubes enables photons to enter more easily, compared to P25- TiO_2 . Also, P25- TiO_2 has higher bandgap energy, as well as a lower surface area of 53.6 m^2/g (Slamet *et al.*, 2017), compared to TNTA, which has lower bandgap energy and a higher surface area of 285 m^2/g (Zhao *et al.*, 2009).

Figure 6 shows the H_2 production (mmol/g) on TNTA-CdS with various CdS loading. During the process, the reactor temperature was measured using a thermocouple and after 75 minutes of irradiation, the temperature was kept constant at about 87°C using exhaust fans. The accumulative hydrogen production on the TNTA, TNTA-CdS-1, TNTA-CdS-2, and TNTA-CdS-3 was approximately 1.503 mmol/g, 1.796 mmol/g, 2.155 mmol/g, and 0.814 mmol/g, respectively. TNTA-CdS-2 produced greater hydrogen, compared to TNTA and TNTA-CdS-1, indicating hydrogen generation increased with an increase in the CdS loading. The highest hydrogen production by TNTA-CdS-2 might be due to the synergy effect of appropriate loading amount and uniformly distributed CdS on TNTA that result in effective separation of h^+ and e^- pairs.

CdS can minimize recombination activity because TNTA has a more positive conduction band (CB), compared to CdS, which causes the electrons to move from the CB of CdS to the CB of TNTA. Meanwhile, CdS has a more negative valence band (VB), compared to TNTA, and consequently, the hole moves from the TNTA VB to the CdS VB. The hole and electron transfer caused differences in the exact locations; therefore, recombination was minimized due to the separation effect (Xu *et al.*, 2018, Zhao *et al.*, 2016) as depicted in Figure 7. Optimal photon absorption was also achieved due to the reduction in the bandgap.

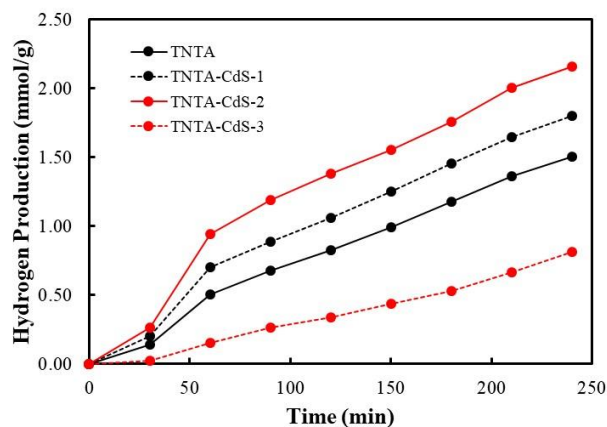


Fig. 6. The relationship between time and hydrogen production on various photocatalysts as a function of irradiation time with an initial 2,4,6-TTCP concentration of 40 ppm.

The enhanced photocatalytic activity up to optimum loading could be due to effective charge transfer, uniformly distributed, strong interaction between CdS and TNTA, responds positively to the visible light, high crystallinity, and large surface area (Elangovan *et al.*, 2021). The presence of CdS also strengthens the mechanical stability and increases the photoanode material's efficiency (Liu *et al.*, 2011). However, TNTA-CdS-3 showed weak performance in hydrogen production. This phenomenon might be due to the presence of an excess CdS loading that causes accumulation of CdS on TNTA surface and has increased particle size which results in the reduction of the surface area since aggregation of CdS causes low dispersion. In another word, the CdS are not dispersed uniformly on the TNTA surface which would reduce the contact area and photocatalytic performance (Elangovan *et al.*, 2021; Zhao *et al.*, 2016). Moreover, smaller CdS quantum dots inject more effectively e^- into TNTA than the bigger ones as reported by Robel *et al.*, 2007 in the previous study. Furthermore, CdS loading greater than optimum conditions could also cause CdS aggregates to become larger and clog the mouth of TNTA (Zhu *et al.*, 2015). Although TNTA-CdS-3 has the strongest absorption indicated by the lowest band gap (2.71 eV), this blocking will affect light absorption in the inner TNTA.

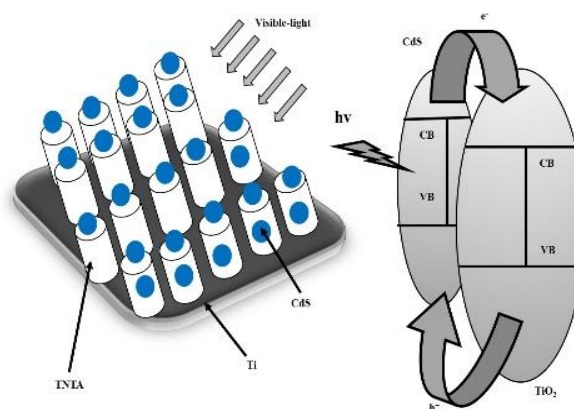


Fig. 7. Electron and hole generation, transfer, and separation between TNTA and CdS in a TNTA-CdS nanocomposite under visible light.

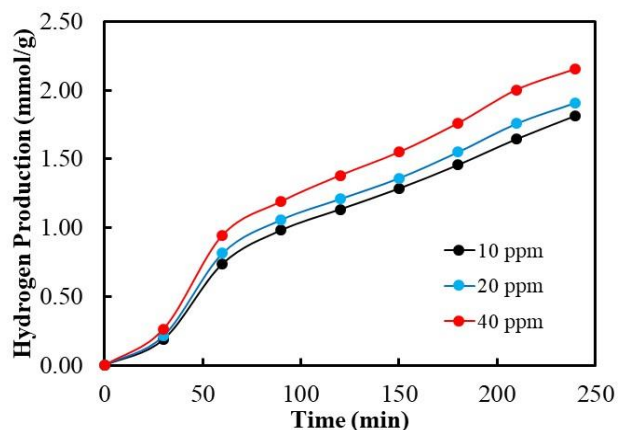


Fig. 8. The relationship between time and H₂ generation at different initial concentrations of 2,4,6-TCP with TNTA-CdS-2 as photocatalyst.

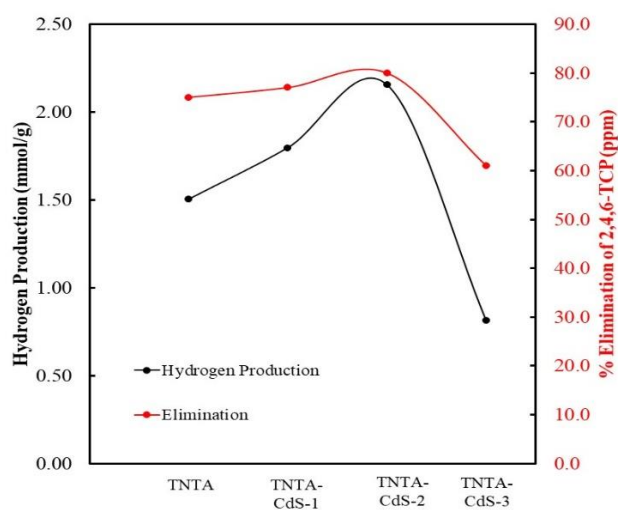
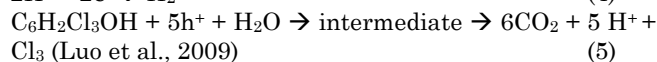
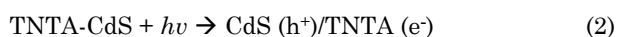


Fig. 9. The synergy effect between 2,4,6-TCP degradation and H₂ generation as a function of various photocatalysts with an initial concentration of 40 ppm and 4 hour-irradiation.

Figure 8 shows the H₂ generation is influenced by the initial concentration of 2,4,6-Trichlorophenol. Increasing in the initial concentration is bound to increase the H₂ produced. At initial concentrations of 10, 20, and 40 ppm, the accumulative H₂ generation was 1.814; 1.910; and 2.155 mmol/g, respectively. This is because 2,4,6 TCP tends to act as a hole scavenger, consequently, minimizing recombination. Also, 2,4,6 TCP is believed to donate H⁺ ions during the reaction, thus, producing more hydrogen (Luo *et al.*, 2009).

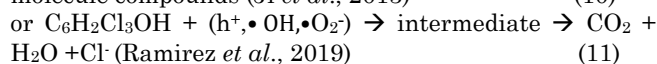
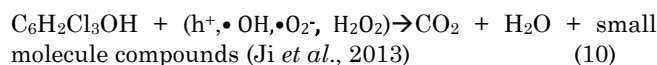
Figure 9 indicates the ability of various photocatalysts in decreasing the concentration of 2,4,6-Trichlorophenol and in producing H₂. The % elimination of 2,4,6-TCP on the TNTA, TNTA-CdS-1, TNTA-CdS-2, and TNTA-CdS-3 was 75, 77, 80, and 61% respectively. Based on the Figure, the % elimination of 2,4,6 TCP is proportional to the H₂ production. The reduction in the concentration of 2,4,6 TPC was due to the conversion into H₂, CO₂, and H₂O by photocatalysis with the possible reaction as in Equation (2) to (11).

The following reaction may be occurred in H₂ production:



If the TNTA-CdS photocatalyst is irradiated with photons ($h\nu$) with energy greater than the bandgap, electron excitation occurs from VB to CB, leaves hole in VB as shown in Figure 7. Hole (h^+) reacts with water and 2,4,6 TCP to produce H⁺, and finally H⁺ is reduced by e⁻ to form hydrogen as presented in Equation (2) to (6).

For the 2,4,6 TCP (C₆H₂Cl₃OH) degradation, the possible pathway could be presented according to Equation (7) to (11).



The oxidizing agent that plays a role in the degradation (h^+ , $\cdot\text{OH}$, $\cdot\text{O}_2^-$, H₂O₂) depends on the photocatalyst used. When TiO₂ is used, $\cdot\text{OH}$ plays a very crucial role in the degradation of 2,4,6-TCP. In contrast, $\cdot\text{O}_2^-$ plays a major role in the degradation if the photocatalyst was MgO-MgFe₂O₄ (Ramirez *et al.*, 2019).

Figure 10 shows the relationship between the elimination of 2,4,6 TCP and the H₂ generation at various initial 2,4,6 TCP concentrations. At the initial concentration of 10, 20, and 40 ppm, the elimination/reduction of the concentration of the pollutants was 9.7, 17.2, and 32 ppm while the accumulative H₂ production was 1.814; 1.910; and 2.155 mmol/g respectively. The elimination of 2,4,6 TCP and the H₂ production was discovered rising, along with an increase on the initial concentration up to 40 ppm. This phenomenon is due to the presence of sufficient or abundant surface area/active site of the TNTA-CdS in absorbing the incident light and the photocatalyst was uniformly distributed. The higher the initial concentration of 2,4,6-TCP up to 40 ppm, the more H₂ is produced and the more 2,4,6-TCP is degraded since the more reactants are degraded and converted.

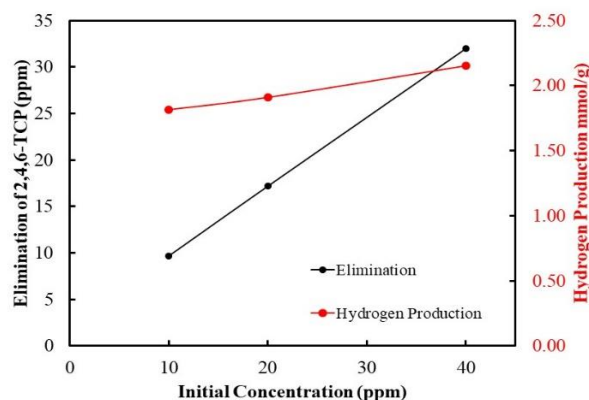


Fig 10. The effect of the initial concentration of 2,4,6-TCP on the elimination of 2,4,6-TCP and hydrogen production (with photocatalyst TNTA-CdS-2, 4 hour-irradiation).

In the H₂ generation mechanism, reactant (2,4,6-TCP) serves as a hole scavenger that increase the H₂ production due to it reducing the recombination of photogenerated electrons-holes. As a result, more electrons reduce H⁺ to generate H₂.

4. Conclusions

TNTA modified with CdS was successfully produced by using the electrodeposition method. According to the SEM images, XRD analysis, and EDX spectra, the CdS nanoparticles were dispersed and deposited on the TNTA surface. The UV-Vis DRS results showed the effect of CdS deposited on TNTA reduced the band gap of TNTA-CdS photocatalyst from 3.10 to 2.71 eV, therefore it shifted to the visible light domain. It indicates the photocatalyst is more responsive to visible light absorption. The deposition CdS on TNTA enabled better electron-hole separation, compared to TNTA alone. However, CdS loading on TNTA more than the optimum condition (TNTA-CdS-2) produced lower photocatalytic activity which is likely due to CdS aggregate clogging the mouth of TNTA that affected light penetration in the inner tube. In addition, excess CdS caused accumulation of CdS on TNTA surface which reduced the contact area. Although TNTA-CdS-3 has the strongest absorption indicated by the lowest band gap (2.71 eV), this blocking would affect light absorption in the inner TNTA. The amount of CdS deposited in TNTA and the initial concentration of 2,4,6 TCP were discovered to influence the performance in photodegradation of 2,4,6 TCP, as well as the hydrogen production. In this study, the TNTA-CdS-2 photocatalyst was found to produce the most optimal hydrogen generation and 2,4,6-Trichlorophenol degradation.

Acknowledgement

This study was financially supported by the program Hibah Riset Dasar no.4/AKM/PNT/2019 Ristek Dikti and cooperation program with the Departement of Chemical Engineering, Universitas Indonesia.

Author Contributions: Ratnawati: Formal analysis, writing, original draft, and validation, Slamet: Conceptualization, methodology, supervision, review-writing, project administration, Farah Diba Toya: Formal analysis, Satrio Kuntolaksono: writing, review, and editing. All authors have read and agreed to the published version of the manuscript.

Funding: This research was funded by the program Hibah Riset Dasar no. 4/AKM/PNT/2019 Ristek Dikti and Universitas Indonesia. The authors received no financial support for the research, authorship, and/or publication of this article.

Conflicts of Interest: The authors declare no conflict of interest.

References

- Acar, C., Dincer, I. & Naterer, G. F. (2016). Review of photocatalytic water-splitting methods for sustainable hydrogen production. *International Journal of Energy Research*, 40(11), 1449-1473. DOI: <https://doi.org/10.1002/er.3549>.
- Ali, M. H. H., Al-Qahtani, K. M., and El-Sayed, S. M. (2019). Enhancing photodegradation of 2,4,6 trichlorophenol and organic pollutants in industrial effluents using nanocomposite of TiO₂ doped with reduced graphene oxide. *Egyptian Journal of Aquatic Research*, 45(4), 321-328. DOI: <https://doi.org/10.1016/j.ejar.2019.08.003>
- Aphairaj, D., Wirunmongkol, T., Pavasupree, S. & Limsuwan, P. (2011). Effect of calcination temperatures on structures of TiO₂ powders prepared by hydrothermal method using thai leucoxene mineral. *Energy Procedia*, 9, 539-544. <https://doi.org/10.1016/j.egypro.2011.09.062>.
- Ba, Q., Jia, X., Huang, L., Li, X., Chen, W. & Mao, L. (2019). Alloyed Pd-Ni hollow nanoparticles as cocatalyst of CdS for improved photocatalytic activity toward hydrogen production. *International Journal of Hydrogen Energy*, 44(12), 5872-5880. <https://doi.org/10.1016/j.ijhydene.2019.01.054>.
- Chen, Z., Dinh, H. N & Miller, E. (2013). *Photoelectrochemical Water Splitting Standards, Experimental Methods, and Protocols*, Springer New York, London.
- Christoforidis, K. C., Syrgiannis, Z., La Parola, V., Montini, T., Petit, C., Stathatos, E., Godin, R., Durrant, J. R., Prato, M. & Fornasiero, P. (2018). Metal-free dual-phase full organic carbon nanotubes/g-C₃N₄ heteroarchitectures for photocatalytic hydrogen production. *Nano Energy*, 50, 468-478. <https://doi.org/10.1016/j.nanoen.2018.05.070>.
- Elangovan, M., Bharathaiyengar, S. M., and Ponnannettiappan, J. (2021). Photocatalytic degradation of diclofenac using TiO₂-CdS heterojunction catalysts under visible light irradiation. *Environmental Science and Pollution Research*, 28, 18186-18200. <https://doi.org/10.1007/s11356-020-11538-w>
- Elysabeth, T., Mulia, K., Ibadurrohman, M., Dewi, E. L. & Slamet. (2021). A comparative study of CuO deposition methods on titania nanotube arrays for photoelectrocatalytic ammonia degradation and hydrogen production. *International Journal of Hydrogen Energy*, 46(53), 26873-26885. <https://doi.org/10.1016/j.ijhydene.2021.05.149>.
- Fu, Y., Qin, L., Huang, D., Zeng, G., Lai, C., Li, B., He, J., Yi, H., Zhang, M., Cheng, M. & Wen, X. (2019). Chitosan functionalized activated coke for Au nanoparticles anchoring: Green synthesis and catalytic activities in the hydrogenation of nitrophenols and azo dyes. *Applied Catalysis B: Environmental*, 255, 117740. <https://doi.org/10.1016/j.apcatb.2019.05.042>.
- Gholipour, M. R., Dinh, C-T., Beland, F. & Do, T-O. (2015). Nanocomposite heterojunctions as sunlight-driven photocatalysts for hydrogen production from water splitting. *Nanoscale*, 7(18), 8187-8208. <https://doi.org/10.1039/c4nr07224c>.
- Hippargi, G., Mangrulkar, P., Chilkalwar, A., Labhsetwar, N. & Rayalu, S. (2018). Chloride ion: A promising hole scavenger for photocatalytic hydrogen generation. *International Journal of Hydrogen Energy*, 43(14), 6815-6823. <https://doi.org/10.1016/j.ijhydene.2017.12.179>.
- Holladay, J. D., Hu, J., King, D. L. & Wang, K. Y. (2009). An overview of hydrogen production technologies. *Catalysis Today*, 139(4), 244-260. <https://doi.org/10.1016/j.cattod.2008.08.039>.
- Ji, H., Chang, F., Hu, X., Qin, W., and Shen, J. (2013). Photocatalytic degradation of 2,4,6-trichlorophenol over g-C₃N₄ under visible light irradiation. *Chemical Engineering Journal*, 218, 183-190. <https://doi.org/10.1016/j.cej.2012.12.033>.
- Junn, Ng. B., Putri, L. K., Kong, X.Y., The, Y.W., Pasbaskhsh, P., Piao, C.S. (2020). Z-Scheme Photocatalytic Systems for Solar Water Splitting. *Advanced Science*, 7, 1-42. <https://doi.org/10.1557/mrs.2010.3>
- Khodadadeh, F., Azar, P. A., Tehrani, M. S., and Assi, N. (2016). Photocatalytic degradation of 2,4,6-Trichlorophenol with CdS nanoparticles synthesized by a microwave-assisted sol-gel method. *International Journal of Nano Dimensions*, 7(3), 263-269. <https://doi.org/10.7508/ijnd.2016.03.010>.
- Khorsandi, H., Ghochlavi, N., and Aghapour, A. A. (2018). Biological degradation of 2,4,6-Trichlorophenol by a sequencing batch reactor. *Environmental Processes*, 5, 907-917. <https://doi.org/10.1007/s40710-018-0333-4>.
- Lavand, A. B. and Malghe Y. S. (2015). Visible light photocatalytic degradation of 4-chlorophenol using C/ZnO/CdS nanocomposite. *Journal of Saudi Society*, 19(5), 471-478. <https://doi.org/10.1016/j.jsocs.2015.07.001>

- Levy, I. K., Mizrahi, M., Ruano, G., Zampieri, G., Requejo, F. G. & Litter, M. I. (2012). TiO₂-photocatalytic reduction of pentavalent and trivalent arsenic: Production of elemental arsenic and arsine. *Environmental Science & Technology*, 46, 2299-2308. DOI: <https://doi.org/10.1021/es202638c>.
- Li, B., Lai, C., Zhang, M., Zeng, G., Liu, S., Huang, D., Qin, L., Liu, X., Yi, F., An, N. & Chen, L. (2020). Graphdiyne: A rising star of electrocatalyst support for energy conversion. *Advanced Energy Materials*, 10(16), 20200177. <https://doi.org/10.1002/aenm.202000177>.
- Li, X., Chen, X., Niu, H., Han, X., Zhang, T., Liu, J., Lin, H. & Qu, F. (2015). The synthesis of CdS/TiO₂ heteronanofibers with enhanced visible photocatalytic activity. *Journal of Colloid and Interface Science*, 452, 89-97. <https://doi.org/10.1016/j.jcis.2015.04.034>.
- Liu, M., Jiao, Y., Zhan, S. & Wang, H. (2020). Ni₃S₂ nanowires supported on Ni foam as an efficient bifunctional electrocatalyst for urea-assisted electrolytic hydrogen production. *Catalysis Today*, 355, 596-601. <https://doi.org/10.1016/j.cattod.2019.05.032>.
- Liu, Y., Zhou, H., Zhou, B., Li, J., Chen, H., Wang, J., Bai, J., Shanguan, W. & Cai, W. (2011). Highly stable CdS-modified short TiO₂ nanotube array electrode for efficient visible-light hydrogen generation. *International Journal of Hydrogen Energy*, 36(1), 167-174. <https://doi.org/10.1016/j.ijhydene.2010.09.089>.
- Luo, H., Zeng, Z., Zeng, G., Zhang, C., Xiao, R., Huang, D., Lai, C., Cheng, M., Wang, W., Xiong, W., Yang, Y., Qin, L., Zhou, C., Wang, H. & Tian, S. (2020). Recent progress on metal-organic frameworks based- and derived- photocatalysts for water splitting. *Chemical Engineering Journal*, 3883, 123196. <https://doi.org/10.1016/j.cej.2019.123196>.
- Luo, N., Jiang, Z., Shi, H., Xiao, T., Edwards, P. P. (2009). Photocatalytic conversion of oxygenated hydrocarbons to hydrogen over heteroatom-doped TiO₂ catalysts. *International Journal of Hydrogen Energy*, 34(1), 125-129. <https://doi.org/10.1016/j.ijhydene.2008.09.097>.
- Mehrpooa, M. & Habibi, R. (2020). A review on hydrogen production thermochemical water-splitting cycles. *Journal of Cleaner Production*, 275, 123836. <https://doi.org/10.1016/j.jclepro.2020.123836>.
- Moreira, T.M.F., Santana, I.L., Moura, M.N., Ferreira, S.A.D., Lelis, M.F.F., Freitas, M.B.J.G. (2017). Recycling of negative electrodes from spent Ni-Cd batteries as CdO with nanoparticle sizes and its application in remediation of azo dye. *Materials Chemistry and Physics*, 195, 19-27. <http://dx.doi.org/10.1016/j.matchemphys.2017.04.009>.
- Park, H., Ou, H-H., Kang, U., Choi, J., Hoffmann, M. R. (2016). Photocatalytic conversion of carbon dioxide to methane on TiO₂/CdS in aqueous isopropanol solution. *Catalysis Today*, 266, 153-159. <https://doi.org/10.1016/j.cattod.2015.09.017>.
- Ramirez, E. R., Tzompantzi-Morales, F., Gutierrez-Ortega, N., Mojica-Calvillo, H. G., and Castillo-Rodriguez, J. (2019). Photocatalytic degradation of 2,4,6-Trichlorophenol by MgO-MgFe₂O₄ derived from layered double hydroxide structures. *Catalysts*, 9, 454. <https://doi.org/10.3390/catal9050454>.
- Ratnawati, Gunlazuardi, J., Dewi, E. L. & Slamet. (2014). Effect of NaBF₄ addition on the anodic synthesis of TiO₂ nanotube arrays photo catalyst for production of hydrogen from glycerol-water solution. *International Journal of Hydrogen Energy*, 39, 16927-16935. <https://doi.org/10.1016/j.ijhydene.2014.07.178>.
- Robel, I., Kuno, M., and Kamat, P. V. (2007). Size-dependent electron injection from excited CdSe quantum dots into TiO₂ nanoparticles. *Journal of the American Chemical Society*, 129(14), 4136-4137. <https://doi.org/10.1021/ja070099a>.
- Sharotri, N. & Sud, D. (2016). Ultrasound-assisted synthesis and characterization of visible light-responsive nitrogen-doped TiO₂ nanomaterials for removal 2-Chlorophenol. *Desalination and Water Treatment*, 57(19), 8776-8788. <https://doi.org/10.1080/19443994.2015.1026278>.
- Shi, Y., Lei, X., Xia, L., Wu, Q. & Yao, W. (2020). Enhanced photocatalytic hydrogen production activity of CdS coated with Zn-anchored carbon layer. *Chemical Engineering Journal*, 393, 124751. <https://doi.org/10.1016/j.cej.2020.124751>.
- Slamet, Ratnawati, Gunlazuardi, J. & Dewi, E. L. (2017). Enhanced photocatalytic activity of Pt deposited on titania nanotube arrays for hydrogen production with glycerol as a sacrificial agent. *International Journal of Hydrogen Energy*, 42(38), 24014-24025. <http://doi.org/10.1016/j.ijhdene.2017.07.208>.
- Slamet^b and Raudina. (2017). Degradation of 2,4,6-Trichlorophenol and hydrogen production simultaneously by TiO₂ nanotubes/graphene composite. *Proceedings of the 3rd International Symposium on Applied Chemistry, AIP Conf. Proc.* 1904, 020074-1-020074-7. <https://doi.org/10.1063/1.5011931>.
- Tian, J., Leng, Y., Zhao, Z., Xia, Y., Sang, Y., Hao, P., Zhan, J., Li, M. & Liu, H. (2015). Carbon quantum dots/hydrogenated TiO₂ nanobelt heterostructures and their broad-spectrum photocatalytic properties under UV, visible, and near-infrared irradiation. *Nano Energy*, 11, 419-427. <https://doi.org/10.1016/j.nanoen.2014.10.025>.
- Tian, S., Zhang, C., Huang, D., Wang, R., Zeng, G., Yan, M., Xiong, W., Zhou, C., M. Cheng, M., Xue, W., Yang, Y. & Wang, W. (2020). Recent progress in sustainable technologies for adsorptive and reactive removal of sulfonamides. *Chemical Engineering Journal*, 389, 123423. <https://doi.org/10.1016/j.cej.2019.123423>.
- Veeraputhiran, V., Gomathinayagam V., Udhaya, A., Francy, K. & Kathrunnisa. (2015) B. Microwave Mediated Synthesis and Characterizations of CdO Nanoparticles. *Journal of Advanced Chemical Sciences*, 1, 17-19.
- Wang, B., He, S., Feng, W., Zhang, L., Huang, X., Wang, K., Zhang, S. & Liu, P. (2018). Rational design and facile in situ coupling non-noble metal Cd nanoparticles and CdS nanorods for efficient visible-light-driven photocatalytic H₂ evolution. *Applied Catalysis B: Environmental*, 236, 233-239. <https://doi.org/10.1016/j.apcatb.2018.05.005>.
- Wang, B., Zhang, L., Chen, Z., Hu, S., Li, S., Wang, Z., Liu, J., and Wang, X. (2014). Semiconductor heterojunction photocatalysts: design, construction, and photocatalytic performances. *Chemical Society Reviews*, 43(15), 5234-5244. <https://doi.org/10.1039/c4cs000126e>.
- Xie, K., Wu, Z., Wang, m., Yu, J., Gong, C., Sun, L. & Lin, C. (2016). Room temperature synthesis of CdS nanoparticle-decorated TiO₂ nanotube arrays by electrodeposition with improved visible-light photoelectrochemical properties. *Electrochemistry Communications*, 63, 56-59. <https://doi.org/10.1016/j.elecom.2015.12.013>.
- Xu, Q., Zhang, L., Yu, J., Wageh, S., Al-Ghamdi, A. A., & Jaroniec, M. (2018). Direct Z-scheme photocatalysts: Principles, synthesis, and applications. *Materials Today*, 21(10), 1042-1063. <https://doi.org/10.1016/j.mattod.2018.04.008>.
- Yu, C., Zhang, Z., Dong, Z. Xiong, Y., Wang, Y., Liu, Y., Cao, X., Dong, W., Liu, M. & Liu, Y. (2021). Fabrication of Heterostructured CdS/TiO₂ Nanotube Arrays Composites for Photoreduction of U(VI) under Visible Light. *Journal of Solid State Chemistry*, 298, 122053. <https://doi.org/10.1016/j.jssc.2021.122053>.
- Zhao, Q., Li, X., Wang, N., Hou, Y., Quan, X. & Chen, G. (2009). Facile fabrication, characterization, and enhanced photoelectrocatalytic degradation performance of highly oriented TiO₂ nanotube arrays. *Journal of Nanoparticle Research*, 11, 2153-2162. <https://doi.org/10.1007/s11051-009-9685-z>.
- Zhao, D. & Feng Yang, C (2016). Recent advances in the TiO₂/CdS nanocomposite used for photocatalytic hydrogen production and quantum-dot-sensitized solar cells. *Renewable and Sustainable Energy Reviews*, 54, 1048-1059. <https://doi.org/10.1016/j.rser.2015.10.100>.
- Zhao, Q., Sun, J., Li, S., Huang, C, Yao, W., Chen, W., Zeng, T. & Xu, Q. (2018). Single nickel atoms anchored on nitrogen-doped graphene as a highly active co-catalyst for photocatalytic H₂ evolution. *ACS Catalysis*, 8(12), 11863. <https://doi.org/10.1021/acscatal.8b03737>.
- Zhao, Y., Huang, X., Gao, F., Tian, Q., Fang, Z-B. & Liu, P. (2019). Study on water splitting characteristics of CdS nanosheets driven by the coupling effect between photocatalysis and

- piezoelectricity. *Nanoscale*, 11(18), 9085-9090. <https://doi.org/10.1039/c9nr01676G>.
- Zheng, Y., Dong, J., Huang, C., Xia, L., Wu, Q., Xu, Q. & Yao, W. (2020). Co-doped Mo-Mo₂C cocatalyst for enhanced g-C₃N₄ photocatalytic H₂ evolution. *Applied Catalysis B: Environmental*, 260, 118220. <https://doi.org/10.1016/j.apcatb.2019.118220>.
- Zhu, Y-P., Ren, T-Z., and Yuan, Z-Y. (2015). Mesoporous phosphorus-doped g-C₃N₄ nanostructured flowers with superior photocatalytic hydrogen evolution performance. *Applied Materials & Interfaces*, 7(30), 16850-16856. <https://doi.org/10.1021/acsami.5b04947>.



© 2022. The Author(s). This article is an open access article distributed under the terms and conditions of the Creative Commons Attribution-ShareAlike 4.0 (CC BY-SA) International License (<http://creativecommons.org/licenses/by-sa/4.0/>)